Probing new physics in the laboratory and in space
Ovchynnikov, M.

Chapter 1

Introduction

In the twentieth century, attempts to explain subatomic physics phenomena combined with two scientific revolutions – special relativity and quantum mechanics – have resulted in the development of the Standard Model of particle physics (SM). The SM successfully describes all the particle physics processes that we observe at accelerators with the help of only 17 particles and interaction between them, that is based on the $SU(3) \otimes SU(2) \otimes U(1)$ gauge group, see Fig. 1.1. The SM has passed a number of precision tests [1–3]. The last stage of the confirmation of SM was the discovery of the Higgs boson at Large Hadron Collider (LHC) [4, 5] and subsequent tests of its properties, which confirmed that it is exactly the same particle as predicted by the SM [6].

> The SM is a closed theory and may be used as an effective theory that makes extremely accurate predictions up to the Planck scale. However, it is not complete. There are a few observational phenomena establishing that SM has to be extended, probably by adding new particles. These phenomena constitute the beyond the SM problems (or BSM problems).

The BSM problems are:

- **Neutrino oscillations**: measurements of solar neutrino flux, as well as observations of atmospheric and collider neutrino interactions, suggest that neutrinos may change their flavor – the phenomenon called neutrino oscillations. The oscillations may occur if neutrinos have different masses. This is not possible in SM, in which neutrinos are massless, but may be resolved by adding interactions with new particles.

- **Dark matter (DM)**: Astrophysical and cosmological observations suggest that most of the mass of the Universe is dominated by a specific type of matter that does not interact with light – the dark matter. The only natural candidate for the role of DM in SM is the SM active neutrino. However, experimental restrictions on neutrino masses make this scenario impossible.
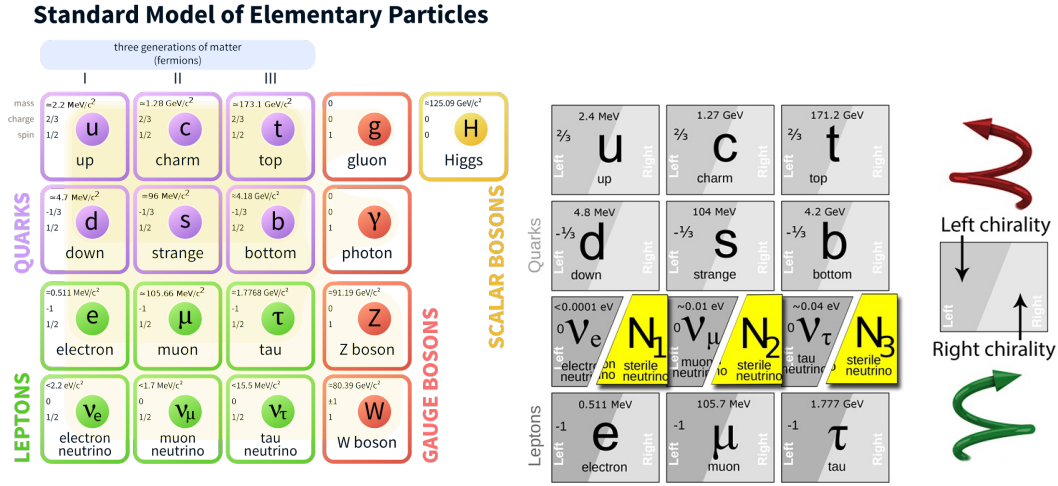
Standard Model of Elementary Particles

Figure 1.1: *Left panel*: The particle content of the Standard model. Twelve elementary particles of matter – leptons, corresponding lepton neutrinos, and quarks – interact with each other via electromagnetic, weak, and strong interactions. The interaction mediators are, correspondingly, a photon, W, Z bosons, and gluons. All of the matter elementary particles except for neutrinos, and W, Z bosons obtain their mass because of the Higgs mechanism. *Right panel*: an extension of the Standard Model with three electrically neutral fermion particles called Heavy Neutral Leptons N. These particles may be capable of solving all three beyond the Standard model phenomena simultaneously.

- **Baryon asymmetry of the Universe**: within the SM, it is impossible to generate the observed asymmetry between matter and antimatter, which is of an order of $10^9 + 1$ baryons per one 10^9 antibaryons.

In order to resolve the BSM problems, one may construct an extension of SM with some new physics particles that are responsible for these phenomena. Unfortunately, they do not provide unique information about the properties of these hypothetical particles, such as spin, mass, and strength of the interaction with different SM particles. As a result, a number of BSM extensions that may resolve the BSM problems is "degenerate": based on the experimental data, we do not have a clear way to choose a particular extension that is realized in nature. This situation is different from the case of the construction of the SM, for which the guideline was provided by a combination of theoretical arguments such as the unitarity and the gauge symmetry, and signatures from the particle physics experiments, that allow determining properties of particles in a unique way.

Currently, there is no signature that tells us uniquely about the properties of new physics particles. Given that a lot of SM extensions may be equally responsible for the resolution of BSM problems, one needs a way to constrain as many models as possible.

1.1 Portals

Non-observation of new physics particles at particle physics experiments may be explained by two reasons: either they are too heavy to be produced at the currently reachable energies, or they are too feebly interacting, such that the intensity of events at the experiment is insufficient to observe them. Further, we will consider the second class of the particles. They are called *Feebly Interacting Particles, or FIPs*.

The FIPs may be directly responsible for the BSM phenomena or serve as mediators between the dark sector and the SM. It is convenient to classify BSM extensions with FIPs by the properties of the particles-mediators:

1. Scalar portal:
$$\mathcal{L} = \alpha_1 H^\dagger H S + \alpha_2 H^\dagger H S^2, \tag{1.1.1}$$

   with H being the SM Higgs doublet, S being a new scalar particle, while $\alpha_{1,2}$ real couplings. Phenomenologically, the scalar S interacts with SM particles in the same way as a light Higgs boson, but the matrix element of any process is suppressed by the mixing angle $\theta \ll 1$. S may play a role of a mediator for the dark sector [7], or be responsible for the inflation by playing the role of an inflaton [8], if having mass in GeV scale.

2. Neutrino portal:
$$\mathcal{L} = F_{\alpha I} \bar{L}_\alpha \tilde{H} N_I + \text{N mass term}, \tag{1.1.2}$$

   where $\tilde{H} = i\sigma_2 H^*$ is the Higgs doublet in the conjugated representation, $L_\alpha = \begin{pmatrix} l_\alpha \\ \nu_\alpha \end{pmatrix}$ is the left SM lepton doublet, N_I Heavy Neutral Leptons (or HNLs), and $F_{\alpha I}$ complex couplings. Phenomenologically, HNLs interact similarly to a SM neutrino ν_α but suppressed by the mixing angle $U_\alpha \ll 1$. HNLs may resolve all of the BSM problems. In particular, to explain neutrino oscillations and the baryon asymmetry of the Universe, we need at least two HNLs with highly degenerate masses, while for DM one needs a long-lived HNL with mass in $\mathcal{O}(\text{keV})$ range. A model with such three HNLs is called Neutrino Minimal Standard Model, or νMSM [9, 10].

3. Vector portal:
$$\mathcal{L} = \frac{\epsilon}{2} F_{\mu\nu} V^{\mu\nu}, \quad \text{or} \quad \mathcal{L} = \epsilon J^\mu V_\mu \tag{1.1.3}$$

   where $F_{\mu\nu}$ is the strength tensor of the gauge field associated with the $U_Y(1)$ gauge group, $V^{\mu\nu}$ is the strength associated with the new vector field V_μ, and J_μ is the conserved SM current (for instance, $B - 3L$ current).

1.2 LHC and dedicated accelerator experiments

During the last few years, particle physics experiments with large events intensity have been proposed to probe FIPs. They are called **Intensity frontier experiments**.

FIPs may interact with SM particles in different ways. In dependence on the type of interaction, different kinds of searching may be preferable. Based on the search type, the Intensity frontier experiments may be classified as follows:

1. **Prompt or displaced visible decays of FIPs:** a possible method to search for unstable FIPs that decays into electrically charged particles is to produce them in collisions of SM particles and then detect their decays into SM particles. Such kind events must be distinguished from pure SM events. For instance, an event with the HNL decay $N \to \mu^- \pi^+$ may be mimicked by a long-lived μ^- and π^+ produced outside the decay volume in some SM process, and whose trajectories closely intersect at one point inside the decay volume. The background reduction is typically reached by preventing the outer particles from reaching the decay volume: either by placing the decay volume far from the collision point (such that SM particles decay before reaching the decay volume), by placing SM particles absorbers/deflectors between the collision point, or by imposing specific events selection criteria that minimize the SM background. Examples include: prompt and displaced searches at the LHC, especially during its high-luminosity phase [11–16]; LHC-based experiments – FASER/FASER2 [17], MATHUSLA [18], Codex-b [19]; experiments at extracted beams – SHiP [20], NA62 in the dump mode (SPS beam at CERN), DUNE near detector [21], DarkQuest [22] (Fermilab).

2. **Rare SM decays:** if decays of FIPs cannot be distinguished from some rare SM processes, one may search for an excess of the corresponding events over the yield predicted by SM. Such rare decays are searched, e.g., at meson factories. Examples include: rare decays of mesons – $B \to K\mu\mu$ at LHCb [23], BaBar [24], and Belle II [25], $K \to \pi\nu\nu$ at NA62 in the kaon mode [26].

3. **Events with missing energy/momentum:** Another class of events is common if FIPs leave detectors invisibly, for instance decaying into uncharged particles. Such type of events may be characterized by a missing energy/momentum. Examples are NA64 [27, 28], Belle, BaBar, which search for the process $e + \text{target} \to e + \text{missing energy}$, and events of the type $p + p \to \text{jet} + \text{missing } p_T$ at the LHC [29–31].

4. **Scatterings of new physics particles:** If being stable, FIPs may still be detected via their scatterings off matter. In this case, the production of FIPs at the laboratory is not necessary, as they could have been generated in the Early Universe and
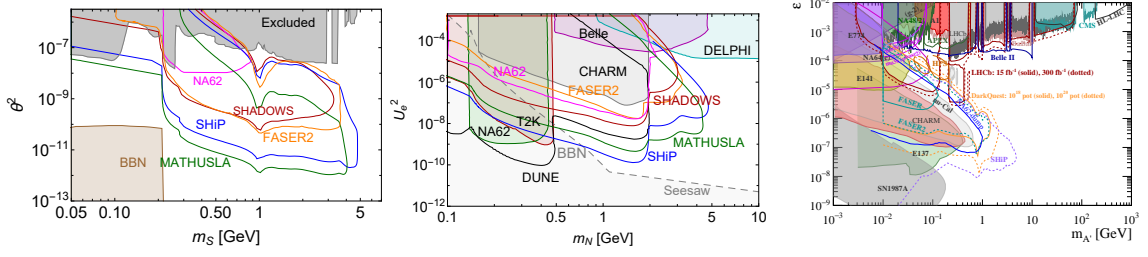
Figure 1.2: Sensitivity reach of Intensity frontier experiment to decays of portal particles: dark scalars (1.1.1) that have zero quartic coupling $HHSS$ (the left panel), Heavy Neutral Leptons (1.1.2) that mix purely with ν_e (the middle panel), and dark photons (1.1.3) (the right panel). The figure for the dark photon and sensitivity contours for HNLs and scalars are given from [36]. The BBN bound for HNLs is reproduced from [37].

surround us today. This may be the case of dark matter particles. Examples of experiments that search for this signature include recently approved SND@LHC [32] and FASERν [33], DUNE near detector, and direct DM detection experiments such as CRESST [34, 35].

The combined sensitivity reach of these experiments to different portal models is shown in Fig. 1.2. We also show there the parameter space excluded by past experiments.

1.2.1 Qualitative comparison of different experiments

Using Fig. 1.2, we may formally compare the potential of different experiments to probe new physics particles. In addition, in order to study principal limitations and advantages of the given experimental setup to probe different new physics models, it would be useful to have a qualitative understanding of the features of the sensitivity.

> The sensitivity of the given experiment to FIPs may be estimated using Monte-Carlo simulations of the number of events. However, this method has several limitations when comparing the sensitivity reach of different experiments.

Indeed, a simulation is typically a "black box" which does not allow us to understand the characteristic features of the sensitivity curve. In addition, it typically costs a huge amount of time and requires a lot of computational resources, which becomes crucial if many simulations are required. This is the case, for instance, during the optimization stage of the experiment, when its design is changed. Another situation is when we change parameters of the FIP model, which requires a new simulation each time.

> A clear, fully controlled estimate of the sensitivity within a factor of few is provided by semi-analytic calculations [9].

Let us consider for instance Intensity frontier experiments that search for visible decays of FIPs X. The number of events at these experiments is given by

$$N_{\text{events}} \approx \sum_i N_i \cdot \text{Br}(i \to X) \cdot \epsilon^{(i)}_{\text{geom}} \cdot P^{(i)}_{\text{decay}} \cdot \text{Br}(X \to \text{vis}) \cdot \epsilon_{\text{decay}} \cdot \epsilon_{\text{rec}} \qquad (1.2.1)$$

Here, N_i is the total number of SM particle species i at the experiment (it may be for instance a particle from the incoming beam, or a secondary particle produced in collisions), $\text{Br}(i \to X)$ is the branching ratio of the process with i which leads to the production of X (it may be a decay or a scattering process), $\epsilon^{(i)}_{\text{geom}}$ is the geometric acceptance – the fraction of particles X that fly in the direction of the detector of the experiment. $P^{(i)}_{\text{decay}}$ is the decay probability:

$$P_{\text{decay}} \approx \exp[-l_{\text{min}}/c\tau_X \gamma^{(i)}_X] - \exp\left[-l_{\text{max}}/c\tau_X \gamma^{(i)}_X\right] \approx$$
$$\approx \begin{cases} l_{\text{fid}}/c\tau_X \gamma^{(i)}_X, & c\tau_X \gamma^{(i)}_X \gg l_{\text{max}} \\ \exp\left[-l_{\text{max}}/c\tau_X \gamma^{(i)}_X\right], & c\tau_X \gamma^{(i)}_X \lesssim l_{\text{min}} \end{cases} \qquad (1.2.2)$$

with $l_{\text{min}}, l_{\text{max}}$ being the minimal and maximal distance defining the decay volume ($l_{\text{fid}} = l_{\text{max}} - l_{\text{min}}$), τ_X the proper lifetime and $\gamma^{(i)}_X$ the mean γ factor. $\text{Br}(X \to \text{vis})$ is the branching ratio of decays of X into visible states (typically, a pair of charged particles). Finally, ϵ_{decay} is the decay acceptance – a fraction of decay products that travel in the direction of the detector, and ϵ_{rec} is the reconstruction efficiency – the fraction of events that are successfully reconstructed in detectors.

The sensitivity curve is defined by the condition $N_{\text{events}} > N_{\text{min}}$, where N_{min} is the number of events required for the detection. The limiting cases in (1.2.2) define the lower and upper bounds of the sensitivity of the experiments shown in Fig. 1.2. Using (1.2.2) together with (1.2.1), we may estimate these bounds analytically. We consider models in which the production and decays of X are controlled by the same coupling g of X to SM, such that $\text{Br}(i \to X), \tau^{-1}_X \propto g^2$. Assuming for simplicity that the production of X is dominated by one specific channel, the scaling of the lower and upper bounds of the sensitivity is given by the following formulas:

$$N_{\text{events,lower bound}} \propto g^4 \Rightarrow g^2_{\text{lower bound}} \sim \sqrt{\frac{N_{\text{min}}}{N_{\text{events,lower bound}}\big|_{g=1}}} \equiv$$
$$\equiv \chi_{\text{lower}} \times \sqrt{\frac{c\tau_X}{\text{Br}(i \to X)\text{Br}(X \to \text{vis})}}\bigg|_{g=1} \qquad (1.2.3)$$

$$N_{\text{events,upper bound}} \propto g^2_{\text{upper}} \exp\left[-l_{\text{min}}/c\tau_X \gamma^{(i)}_X\right] \Rightarrow g^2_{\text{upper}} \sim \frac{\gamma^{(i)}_X}{l_{\text{min}}c\tau_X}\bigg|_{g=1} \equiv \chi_{\text{upper}} \cdot \frac{1}{c\tau_X}\bigg|_{g=1},$$
$$(1.2.4)$$

Here, we have separated the experiment-independent parameters, which cancel out when comparing different experiments, from the experiment-specific quantities:

$$\chi_{\text{lower}} \equiv \sqrt{\frac{N_{\min} \cdot \gamma_X^{(i)}}{N_i \cdot \epsilon_{\text{geom}}^{(i)} \cdot l_{\text{fid}} \cdot \epsilon_{\text{decay}} \cdot \epsilon_{\text{rec}}}}, \quad \chi_{\text{upper}} \equiv \frac{\gamma_X^{(i)}}{l_{\min}} \qquad (1.2.5)$$

> The lower and upper bounds of the sensitivity of the Intensity frontier experiments may be estimated with the help of several geometric parameters.

We are now ready to compare the lower and upper bounds of different experiments. We consider the following experiments: MATHUSLA and FASER2 at the LHC, and SHiP and SHADOWS at SPS, and restrict the masses of FIPs by the GeV range. Their parameters are summarized in Table 1.1.

Experiment	SHiP	SHADOWS	MATHUSLA	FASER2
$\sqrt{s}$, GeV	28	28	13000	13000
N_{PoT}	$2 \cdot 10^{20}$	$\sim 5 \cdot 10^{19}$	$2.2 \cdot 10^{17}$	$2.2 \cdot 10^{17}$
$\frac{l_{\min}}{\text{m}}$	50	10	40	480
$\frac{\langle l_{\text{fid}} \rangle}{\text{m}}$	50	20	100	5
$\frac{\theta_{\text{det}}}{\text{rad}}$	$(0, 0.025)$	$(0.03, 0.09)$	$(0.48, 0.9)$	$(0, 2.1 \cdot 10^{-3})$

Table 1.1: Parameters of different Intensity frontier experiments: the beam CM energy $\sqrt{s}$, the total number of the proton-proton collisions expected during the working period N_{PoT}, the distance to the beginning of the decay volume $l_{\min}$, the average length of the decay volume $\langle l_{\text{fid}} \rangle$, polar angle coverage of detectors θ_{det}.

We consider three different production channels: proton bremsstrahlung, that is important for dark photons and dark scalars, decays of D mesons, which are important for HNLs, and decays of B mesons, which are important for dark scalars and HNLs [38, 39], see Fig. 1.3. We adopt the description of the probabilities of these channels from [38, 39]. For particles from decays of mesons, we approximate the kinematic quantities such as γ_X and ϵ_{geom} by the corresponding quantities of mesons. This is a meaningful approximation since the angular distribution differs only by the quantity $\Delta\theta \simeq m_{B,D}/E_{B,D}$, which is typically much smaller than the angular coverage of the experiments of interest. We use the total amount and spectra of D, B mesons at the LHC provided by the FONLL package [40–43] and at SPS by [44]. Finally, we estimate ϵ_{decay} with the help of a simple Monte-Carlo simulation.[1]

Let us now highlight important points relevant for the comparison:

---

[1]We require decay products from two-body decays of particles with masses $m_{B/D}$ for decays from B/D mesons and 1 GeV for the production by bremsstrahlung to point to detectors.
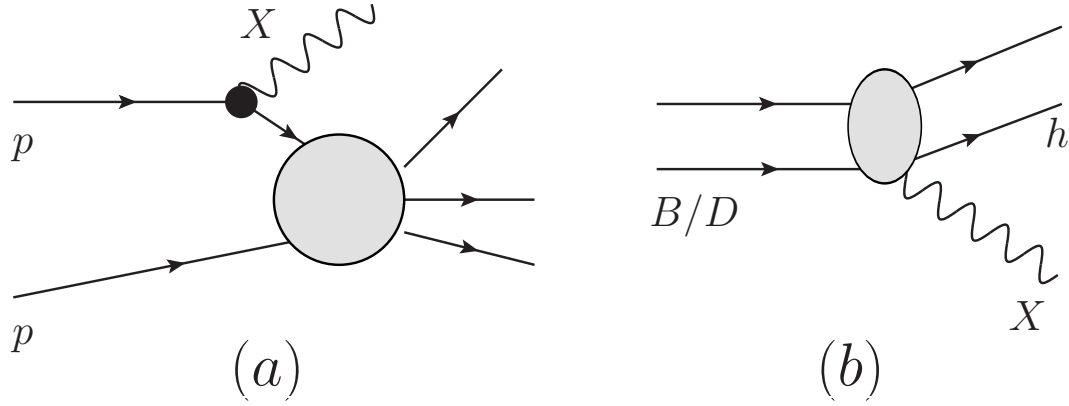
Figure 1.3: Typical production channels for a FIP X that has mass in $\mathcal{O}(\text{GeV})$ range: proton bremsstrahlung (the diagram (a)), and decays of B, D mesons into a FIP and other particle h (the diagram (b)).

1. Particles produced by the proton bremsstrahlung have small transverse momenta $p_T \lesssim \Lambda_{\text{QCD}}$ and hence are very collimated with respect to the beam axis. Therefore, off-axis experiments like SHADOWS and MATHUSLA do not have the sensitivity to this channel.

2. For the production from mesons, the invariant mass of collisions $\sqrt{s}$ must be much larger than the doubled mass of meson; otherwise, the meson production probability gets suppressed. As a result, at the SPS beam energy, the fraction of produced B mesons per one proton-proton collision is $\simeq$ few $\cdot 10^{-7}$, since $2m_B \approx 10$ GeV is not too far from $\sqrt{s_{\text{SPS}}} \approx 28$ GeV. At the LHC, $\sqrt{s} = 13$ TeV, and the probability is much higher, reaching 10^{-2}. For D mesons, there is no such significant difference, as their mass is significantly lower. However, the suppression at SPS is compensated by a much larger beam intensity.

3. The distribution of B, D mesons is collimated, although not so strong as compared to the bremsstrahlung. This leads to much lower (but non-zero) geometric acceptance for the off-axis experiments. As a result of these factors, the amounts of B mesons at SHiP, FASER2, and MATHUSLA are comparable, while at SHADOWS it is even suppressed.

4. Experiments located close to the beam collision point, such as SHADOWS, may have an advantage at the upper bound of the sensitivity even despite lower average momentum. On-axis experiments at the LHC such as FASER2, although being located far away from the collision point, are still competitive at the upper bound due to large average momenta of particles produced in energetic beams collisions in the far-forward direction.

The resulting parameters (1.2.5) are summarized in Table 1.2.

Experiment	SHiP	SHADOWS	MATHUSLA	FASER2
$N_{\min}$	3	3	3	3
$N_B \cdot \epsilon_{\text{geom}}^B$	$8 \cdot 10^{13}$	$5 \cdot 10^{11}$	$3 \cdot 10^{13}$	10^{13}
$N_D \cdot \epsilon_{\text{geom}}^D$	$8 \cdot 10^{17}$	$2 \cdot 10^{16}$	$5 \cdot 10^{14}$	$2 \cdot 10^{14}$
$N_{\text{PoT}} \cdot \epsilon_{\text{geom}}^{\text{brem}}$	10^{20}	–	–	$2 \cdot 10^{16}$
$\epsilon_{\text{decay}, B}$	0.4	< 0.4	$\mathcal{O}(1)$	$\mathcal{O}(1)$
$\epsilon_{\text{decay}, D}$	0.4	$\simeq 0.3$	$\mathcal{O}(1)$	$\mathcal{O}(1)$
$\epsilon_{\text{decay}, \text{brem}}$	$\mathcal{O}(1)$	–	–	$\mathcal{O}(1)$
$\chi_{\text{lower}, B}$	$4 \cdot 10^{-7}$	$6 \cdot 10^{-6}$	10^{-7}	$2 \cdot 10^{-6}$
$\chi_{\text{lower}, D}$	$3 \cdot 10^{-9}$	$8 \cdot 10^{-8}$	$4 \cdot 10^{-8}$	$5 \cdot 10^{-7}$
$\chi_{\text{lower}, \text{brem}}$	10^{-10}	–	–	10^{-7}
$\chi_{\text{upper}, B}$	2	6	0.1	3
$\chi_{\text{upper}, D}$	1	2	0.03	2
$\chi_{\text{upper}, \text{brem}}$	3	–	–	2

Table 1.2: Potential reach of different Intensity frontier experiments as predicted by Eqns. (1.2.5). The relevant parameters $N_{B,D}, \epsilon_{\text{geom}}, \epsilon_{\text{decay}}$. The minimal number of events required for the discovery, $N_{\min}$, corresponds to the assumption of absence of background at 95% CL.

From the discussion, we conclude that SHiP is the most powerful "non-compromised" experiment proposed to search for FIPs with masses below 5 GeV.

1.3 Astrophysical and cosmological probes: defining the parameter space of interest for accelerator experiments

Searches for FIPs at accelerator experiments are restricted by short-lived particles. The upper bound on lifetimes that may be constrained is model-dependent. For instance, for HNLs it may be as large as $\tau_N \simeq 10^{-2}$ s at masses $m_N > 0.5$ GeV, see Fig. 1.4. It is therefore important to define the target parameter space of FIPs to be probed by the accelerator experiments.

Signatures that may be sensitive to long-lived FIPs are cosmological and astrophysical observables.

In the Early universe or inside a dense medium of a supernova, the intensity of collisions was much higher than at colliders. Therefore, despite tiny couplings to the SM particles, FIPs may be produced in amounts significant enough to potentially alter the cosmological observables.
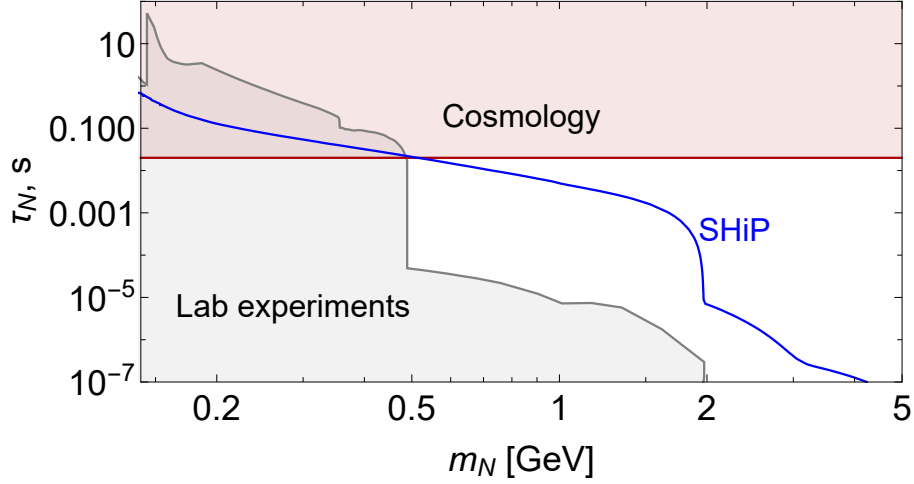
Figure 1.4: The complementarity of FIP signatures coming from past laboratory experiments and cosmological observations, demonstrated using a particular FIP example – HNLs with the pure e mixing. Laboratory experiments are able to probe the parameter space of relatively short-lived particles, whereas cosmological observations such as Big Bang Nucleosynthesis and Cosmic Microwave Background may rule out long-lived HNLs. Together, they define the target parameter space for future experiments such as SHiP.

Cosmological and astrophysical probes include: abundances of primordial light elements synthesized during Big Bang Nucleosynthesis (BBN); the spectrum of Cosmic Microwave Background (CMB); galactic X-ray lines; supernova explosion observation; primordial magnetic fields. The experimental status of these observations is different. For instance, while the CMB spectrum is measured very accurately, the supernova evolution is probed poorly, as it is based on only one observation of the explosion of SN1987A.

Predictions for these observables based on the standard cosmological model (Λ Cold Dark Matter, or ΛCDM) and only SM particles populating the plasma do not contradict the measurements. By adding a new particle, we may break this agreement.

Cosmological probes that may constrain the shortest FIPs lifetimes are BBN and CMB. They may be affected by FIPs with lifetimes as small as $\tau_{\text{FIP}} \simeq 0.01$ s.

The earliest probe from the Early Universe is BBN. BBN is sensitive to the evolution of the Universe at cosmological times as small as $t \simeq \mathcal{O}(1 \text{ s})$, when neutrons decouple from the primordial plasma (see subsection 1.3.1 below). As their decoupling is not instantaneous, the population of neutrons at decoupling is sensitive to the dynamics at even earlier times. In particular, it may constrain particles with lifetimes as small as $\tau_{\text{FIP}} \gtrsim 0.01$ s (see Sec. 1.3.1). Another probe is CMB: although it is associated to the epoch at which electrons and protons get bounded into the Hydrogen atom, its characteristic features (i.e., the angular horizon or the damping scale) depend on the primordial helium abundance and the effective number of

relativistic degrees of freedom, N_{eff}, which, in their turn, are determined by the evolution of the Universe at time scales as small as $t \simeq 0.1$ s. Below, we discuss them in more detail.

1.3.1 BBN

There are two cosmic sources of chemical elements: the evolution of stars, and the primordial evolution of the Universe, which is assumed initially to be hot and/or ultra-dense, thus having conditions for nucleosynthesis. The primordial abundances may be measured in star-poor regions. If the primordial nuclear synthesis was in equilibrium, we would expect that the present Universe is dominated by iron, as it has the largest binding energy per nucleon and therefore is thermodynamically favorable. However, the measurements have indicated the existence of only light elements up to ^{7}Li. This leads us to the conclusion that nuclear reactions were not in thermodynamical equilibrium.
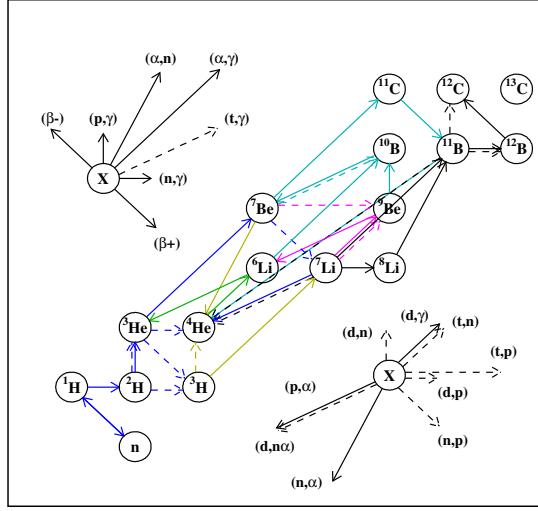

Figure 1.5: The chain of primordial nuclear reactions adopted from [45].

A natural explanation of this feature has been given by Gamow in 40-ties. He assumed that the Universe was hot and radiation dominated during BBN rather than cold and ultradense, which implies a small baryon-to-photon ratio, $\eta_B = n_B/n_\gamma \ll 1$. In the thermal medium, two-particle reactions are much more probable than other multi-body processes. Therefore, the first reaction in the nuclear chain is the deuterium synthesis process $p + n \to d + \gamma$, see Fig. 1.5. At temperatures larger than the binding energy of deuterium nuclei, $T > \Delta_D$, BBN was not efficient because synthesized nuclei were immediately destroyed by photons (that have average energy $E_\gamma \simeq T$). The temperature of the onset of nuclear reactions, T_{BBN}, may be estimated as a temperature at which the number density of photons with energies higher than the deuterium binding energy, $E_\gamma > \Delta_D = 2.2$ MeV, became comparable with the number density of nucleons:

$$n_{\gamma, E_\gamma > \Delta_D}(T_{\text{BBN}}) \simeq n_B(T_{\text{BBN}}) = \eta_B n_\gamma(T_{\text{BBN}}), \tag{1.3.1}$$

which implies $T_{\text{BBN}} \simeq \Delta_D / \ln(\eta_B^{-1}) \sim 0.1\Delta_D \simeq 100\,\text{keV}$. At such low temperatures, however, heavy elements cannot be formed because of the Coulomb barrier. Indeed, the probability of the synthesis process $X_1 + X_2 \rightarrow X_3$, with X_i being some nucleus with mass and charge m_i and Z_i, is suppressed by the Coulomb repulsion factor

$$\sigma v \propto e^{-\eta}, \quad \eta = \frac{Z_1 Z_2 \alpha_{\text{EM}}}{v(T)} = \frac{Z_1 Z_2 \alpha_{\text{EM}}}{\sqrt{T}} \frac{\sqrt{m_1 m_2}}{\sqrt{m_1} + \sqrt{m_2}}, \tag{1.3.2}$$

The synthesis effectively does not occur if

$$\eta(T_{\text{BBN}}) \gtrsim 1 \Rightarrow T_{\text{BBN}} \lesssim T_{\text{coulomb}} = \frac{m_1 m_2 Z_1^2 Z_2^2}{(\sqrt{m_1} + \sqrt{m_2})^2} \tag{1.3.3}$$

As a result, using $T_{\text{BBN}} \simeq 100\,\text{keV}$, we conclude that no nucleus heavier than ^{12}C may be synthesized efficiently (^{12}C is produced in the process $^4\text{He} + ^8\text{Be} \rightarrow ^{12}\text{C} + 2\gamma$, for which $T_{\text{coulomb}} \simeq T_{\text{BBN}}$).

The only robust measurements of primordial abundances are those of d and ^4He.

Indeed, the ^3He isotope is measured only in regions with high metallicity, and it is not possible to estimate the effect of the stellar evolution on its abundance [46]. The measurements of ^7Li [47] set the lower bound on the primordial abundance since ^7Li might be destroyed in low-metallicity stars.

The abundance of the primordial ^4He, Y_p, is measured by three ways: *(i)* the low-metallicity extragalactic method, according to which the helium abundance is measured in low-metallicity regions and then extrapolated to zero metallicity; *(ii)* the intergalactic method – measurements of Y_p in the low-metallicity extragalactic gas; and *(iii)* the CMB method, for which the helium abundance is extracted from the CMB damping tail. The current error in the determination of ^4He at 1σ is around 4% (see Sec. 3.1.1).

In the Standard Model BBN (or SBBN), the only free parameter is η_B.

Using the value of η_B measured from CMB, we find that the predictions of SBBN agree with measurements of d and ^4He [48]. Therefore, to understand the impact of FIPs on BBN, we should first learn SBBN.

The SBBN proceeds as follows. Above T_{BBN}, we have only $p, n, e^{\pm}, \nu, \bar{\nu}, \gamma$ particles in the plasma. During the whole BBN, ultrarelativistic particles dominate the energy density of the Universe and determine the dynamics of the expansion of the Universe and hence the Hubble rate H. $e^{\pm}, \nu, \bar{\nu}$, in addition, keep protons and neutrons in thermal equilibrium by weak reactions

$$p + \bar{\nu} \leftrightarrow n + e^+, \quad n + \nu_e \leftrightarrow p + e \tag{1.3.4}$$

at large temperatures $T \gg 1$ MeV, such that $n_n/n_p = e^{-(m_n - m_p)/T}$. However, neutrons decouple at some temperature of order $T_{\text{dec}} \simeq 1$ MeV, determined by the condition

$$\Gamma_{p \leftrightarrow n}(T_{\text{dec}}) \simeq H(T_{\text{dec}}), \tag{1.3.5}$$

where $\Gamma_{p \leftrightarrow n}$ is the $p \leftrightarrow n$ conversion rate. Afterwards, the population of neutrons evolves due to free decays only, $n \to e + p + \bar{\nu}_e$, with the neutron lifetime $\tau_n \approx 880$ s.

At temperatures around T_{BBN}, the number density of photons with $E_\gamma < \Delta_D$ drops below n_B, and the synthesis starts. Among all light elements which may be synthesized, remind Eq. (1.3.3), helium has the largest binding energy per nucleon. Therefore, its abundance may be estimated from the assumption that all free neutrons got bound in ^{4}He:

$$Y_p = \frac{m_{^4\text{He}} n_n}{m_B(n_n + n_p)} \bigg|_{T=T_{\text{BBN}}} \simeq \frac{n_n/n_p}{n_n/n_p + 1} \bigg|_{T=T_{\text{dec}}} \cdot e^{-t(T_{\text{BBN}})/\tau_n} \tag{1.3.6}$$

The amounts of other elements is not possible to estimate analytically in accurate way, as the BBN dynamics is not equilibrium. In addition, the estimate of the helium abundance based on Eq. (1.3.5) is very sensitive to T_{dec}, since it assumes the instant decoupling of neutrons and therefore T_{dec} enters the exponent in $n_n/n_p|_{T=T_{\text{dec}}} = e^{-(m_n - m_p)/T_{\text{dec}}}$. Therefore, in order to obtain precise values predicted by SBBN, one has to solve the system of Boltzmann equations for nuclear abundances (see, e.g. [48] and references therein).

1.3.1.1 How short-lived FIPs affect BBN

Let us now assume that in addition to SM particles we also have FIPs in the plasma. We are interested in the lower bound on lifetimes for which BBN may be affected. Therefore, we consider "small" lifetimes $\tau_{\text{FIP}} \ll 1$ s, where the time scale is given by the rough time of the neutron/neutrino decoupling. The most part of such short-lived FIPs decay at times $t \lesssim \tau_{\text{FIP}}$ (i.e. at temperatures when neutrinos and neutrons are in perfect equilibrium), and thus does not affect BBN. The BBN is changed by the residual population of FIPs that survive at times $t \gtrsim \tau_{\text{FIP}}$, which is exponentially suppressed.[2] FIPs may affect the dynamics of BBN via the following mechanisms:

1. Change the dynamics of the expansion of the Universe. Before FIPs decay, the energy density of heavy FIPs with $m_{\text{FIP}} \gg T$ may contribute significantly to the total energy density of the Universe, as the ratio of the energy density of non-relativistic relics to the energy density of SM species scales as $\rho_{\text{FIP}}/\rho_{\text{SM}} \propto m_{\text{FIP}}/T$. The largeness of the ratio m_{FIP}/T may partially compensate the exponential suppression of the population of FIPs at times $t \gtrsim \tau_{\text{FIP}}$, and effects of the energy density may not be neglected. Decays of remaining FIPs into neutrinos and EM particles reheat them, in general

---

[2]Further, we assume that the value of η_B after the disappearance of FIPs from the plasma is given by the value predicted by CMB. This assumption is reasonable since we cannot extract η_B from earlier measurements.

differently. This leads to a change of the number of the ultrarelativistic degrees of freedom, $N_{\rm eff}$:

$$N_{\rm eff} = \frac{4}{7}\left(\frac{11}{4}\right)^{\frac{4}{3}}\frac{\rho_\nu}{\rho_\gamma} \tag{1.3.7}$$

and thus the Hubble rate at times $t > \tau_{\rm FIP}$, which affects the dynamics of BBN.

2. Change the $p \leftrightarrow n$ conversion reactions. This may happen for instance if FIPs decay into neutrinos at temperatures $\mathcal{O}(1\,{\rm MeV})$. Since neutrinos are not in perfect equilibrium at these temperatures [49], decays of FIPs change the shape of their distribution function, which affects the neutron-to-proton ratio via the conversion processes (1.3.4). Another example is long-lived mesons such as $\pi^\pm/K$, which, being produced by FIPs, convert $p \leftrightarrow n$ via strong interactions:

$$\pi^- + p \to n + \gamma, \quad \pi^+ + n \to p + \gamma, \quad K^- + p/n \to n/p + X \tag{1.3.8}$$

> If FIPs decay into mesons, the lower bound on lifetimes that may be constrained by BBN comes from the effect of the meson-driven $p \leftrightarrow n$ conversion.

Indeed, the cross sections the processes (1.3.8) are many orders of magnitude larger than the weak $p \leftrightarrow n$ conversion cross-section:

$$\frac{\sigma_{p\leftrightarrow n}^{\rm strong}}{\sigma_{p\leftrightarrow n}^{\rm weak}} \sim \frac{m_p^{-2}}{G_F^2 T^2} \sim 10^{-16}\left(\frac{1\,{\rm MeV}}{T}\right)^2, \tag{1.3.9}$$

Therefore, if FIPs decay into mesons, even their tiny amount comparable with the baryon number density (i.e., much smaller than the neutrino number density) may significantly affect the dynamics of the n/p ratio. The situation is different for the effects via neutrino spectral distortions and the expansion of the Universe. In the latter cases, the energy density of FIPs has to contribute non-negligible to the energy density of the Universe, which requires a much larger number density of FIPs than in the case of mesons.

1.3.2 CMB

In the primordial Universe, protons, electrons and photons were connected to each other via EM interactions, constituting the EM plasma. The hydrogen atom synthesis process,

$$p + e \to H + \gamma, \tag{1.3.10}$$

was much less efficient than the dissociation process

$$\gamma + H \to p + e \tag{1.3.11}$$

driven by the plasma photons. However, as temperature dropped to values around $T \simeq 1$ eV (or redshifts $z_* \simeq 1100$), the amount of photons with energies large enough to dissociate the hydrogen dropped below the baryon number density n_B. As a result, electrons and protons got bounded into H, and the primordial plasma became transparent for photons. These primordial photons survive until our times in the form of CMB.

At large scales, the CMB spectrum is nearly homogeneous and isotropic and well-described by the Planck distribution with the temperature $T_{\text{CMB}} = 2.7255 \pm 0.0006$ K [50], which is one of the confirmations of the Big Bang theory. Interesting physics is hidden in its perturbations.

Let us introduce the variation of the temperature $\delta T(\mathbf{n}) = (T(\mathbf{n}) - T_{\text{CMB}})/T_{\text{CMB}}$, and expand it in terms of spherical harmonics Y_{lm}:

$$\delta T(\mathbf{n}) = \sum_{l,m} a_{lm} Y_{lm}(\theta, \phi), \tag{1.3.12}$$

where $\mathbf{n}(\theta, \phi)$ is the unit vector defining the direction on the sky. To characterize the inhomogeneities, we introduce the autocorrelation function

$$C(\theta) = \langle |\delta T(\mathbf{n}_1)\delta T(\mathbf{n}_2)| \rangle, \quad \cos(\theta) = \mathbf{n}_1 \cdot \mathbf{n}_2 \tag{1.3.13}$$

Using Eq. (1.3.12), we obtain

$$C(\theta) = \frac{T_{\text{CMB}}^2}{4\pi} \sum_l (2l+1) C_l P_l(\cos(\theta)) \tag{1.3.14}$$

Here, we have assumed that the coefficients a_{lm} satisfy the relation

$$\langle a_{lm}^* a_{l'm'} \rangle = C_l \delta_{mm'} \delta_{ll'} \tag{1.3.15}$$

The monopole component of the CMB, C_0, gives us the information about the CMB temperature T_{CMB}. The dipole component C_2 comes from the relative motion of the Solar system with respect to the CMB radiation frame, which results in the Doppler shift (with $\beta = v/c$ being the β factor of the relative motion)

$$T(\theta) \approx T_\gamma (1 + \beta \cos(\theta) + \mathcal{O}(\beta^2)) \tag{1.3.16}$$

Multi-poles $C_l, l \geq 2$ provide us information about primordial perturbations of the power spectrum. They are shown in Fig. 1.6.

> The main characteristic features of the CMB anisotropy spectrum from Fig. 1.6 are inhomogeneities in the CMB temperature of order $\delta T/T_{\text{CMB}} \simeq 10^{-5}$, the presence of oscillations for $l \gtrsim 100$, their exponential suppression at scales $l \gtrsim 10^3$.
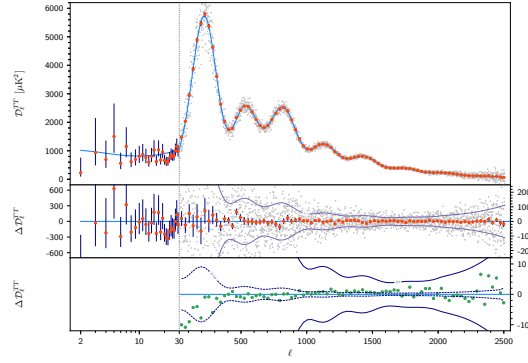
Figure 1.6: The CMB power spectrum measured by PLANCK 2018 [51]. The light blue curve corresponds to the best-fit spectrum in ΛCDM.

Qualitatively, the peaks at multipoles $l \gtrsim 100$ result from acoustic oscillations of the matter density. They originate from the competition between the pressure of photons and the gravitational pressure of matter which tries to form potential wells. There are three characteristics we can extract from the peaks:

1. Their relative height. Odd peaks correspond to compression of acoustic waves, even peaks to rarefaction. If we were to fix everything but increase the baryon density, the compression peaks (first, third, fifth, etc.) would increase in height relative to the rarefaction peaks (second, fourth, sixth, etc.). As a result, the ratio of the second to first peak amplitude tells us about the baryon density. The third peak is located at smaller scales when the Universe was more radiation-dominated. The abundance of DM alters when radiation domination stops and DM potential wells can grow. This then determines how much the sound waves can compress. The height of the third peak relative to the first or second peak thus tells us about the time of matter-radiation equality (and therefore matter density).

2. Their position as a function of angular scale. The most prominent one is the first peak and corresponds to the sound horizon r_s – the distance sound waves have traveled before recombination:

$$r_\mathrm{s} = \int c_\mathrm{s} \frac{da}{a^2 H}, \qquad (1.3.17)$$

where $c_\mathrm{s} = \left[3 \left(1 + \frac{3\rho_\mathrm{b}}{4\rho_\gamma} \right) \right]^{-1/2}$ is the velocity of the sound waves. The corresponding angular scale is $\theta_\mathrm{s} = r_\mathrm{s}/D_A$, where $D_A = \int_{z_\mathrm{eq}}^{0} dz/H(z)$. Since T_CMB (and thus ρ_γ) has been measured, the sound speed only depends on the baryon energy density. Based on measurements of the location of this peak, one can deduce that $\Omega_\mathrm{m} + \Omega_\Lambda = 1$, i.e., the Universe is flat.

21

3. Their damping at smaller angular scales. Photons have a mean free path, diffuse and thus mix hot regions with cold regions. This leads to a dampening of small-scale fluctuations that goes as $\exp(-r_{\mathrm{d}}^2/\lambda^2)$, where r_{d} is the damping scale:

$$r_{\mathrm{d}}^2 = \int \frac{\mathrm{d}a}{a^3 \sigma_{\mathrm{T}} n_e H} \left(\frac{R^2 + \frac{16}{15}(1+R)}{6(1+R^2)} \right) \,, \tag{1.3.18}$$

where $R = 3\rho_{\mathrm{b}}/4\rho_\gamma$. Note here that $r_{\mathrm{d}} \propto H^{-1/2}$.

1.3.2.1 Impact of short-lived FIPs on CMB

Short-lived FIPs with $\tau_{\mathrm{FIP}} \ll 1$ s do not survive until the recombination and thus do not directly affect CMB. However, they may change populations of neutrinos and photons, and also affect the primordial helium abundance, which changes properties of CMB.

We may parametrize the first effect via a change in N_{eff}, see Eq. (1.3.7). In general, it affects many parameters important for CMB: examples are sound horizon and damping scale $r_{\mathrm{s}}, r_{\mathrm{d}}$ discussed in the previous subsection, and the redshift z_{eq} of the radiation-matter equality. It is non-trivial to estimate the impact of the first effect on CMB, as it may be mimicked by variations of other cosmological parameters [52]. To characterize the less degenerate impact, it is possible to make a rescale of cosmological parameters which leaves $\theta_{\mathrm{s}} = r_{\mathrm{s}}/d_A, z_{\mathrm{eq}}$ invariant [53]. Under such a rescale, the remained impact of N_{eff} is on the damping scale, $\theta_d \propto (1 + 0.22 N_{\mathrm{eff}})^{\frac{1}{4}}$ (see also also [54]).

Even in these conditions, N_{eff} is still, however, degenerate with the other parameter changed by FIPs – the primordial helium abundance Y_p. The degeneracy appears since r_{d} depends on the amount of free electrons, which at low temperature is given by the proton abundance, $r_{\mathrm{d}} \sim n_e^{-1} \sim 1/\sqrt{1 - Y_p}$. Therefore,

$$\theta_d \propto \frac{(1 + 0.22 N_{\mathrm{eff}})^{\frac{1}{4}}}{\sqrt{1 - Y_p}} \tag{1.3.19}$$

The effect caused by a change in N_{eff} which is non-degenerate with ΛCDM parameters is the change of the CMB damping scale given by Eq. (1.3.18). There is, however, a degeneracy between N_{eff} and the helium abundance Y_p.

Marginalizing over the value of Y_p, the current bounds imposed by CMB on N_{eff} is $N_{\mathrm{eff}} = 2.89 \pm 0.62$ at 2σ [55].

1.4 Summary

In the lack of explanations of several phenomena in particle physics, the Standard model requires to be extended, probably by adding new particles. However, from current observations, we do not have a clear guideline on the choice of this extension. Therefore, it is reasonable to search for new particles in as much model-independent way as possible.

The work described in this thesis is devoted to a study of two different signatures of new physics particles: their search at future particle physics experiments, and their impact on different cosmological observables. They are complementary to each other, with the first one allowing to probe the parameter space of short particle lifetimes, and the second one constraining large lifetimes. In Chapter 2, we study different signatures with new physics particles at laboratory experiments: their decays the past experiment CHARM (Sec. 2.1) and at displaced vertices at the LHC (Sec. 2.2), and their scatterings at SND@LHC (Sec. 2.3). In Chapter 3, we study the impact of short-lived particles on cosmological observations. Namely, we consider the bounds on particles decaying hadronically on BBN in Sec. 3.1, and the effect of short-lived particles on N_{eff} in Sec. 3.2. We then apply these results to derive the constraints on HNLs in Sec. 3.3.1.